Available online at www.sciencedirect.com

ScienceDirect

journal homepage: www.elsevier.com/locate/he

High-performance Ru-based electrocatalyst composed of Ru nanoparticles and Ru single atoms for hydrogen evolution reaction in alkaline solution

Jin Peng [a], *Yinghuan Chen* [a], *Kai Wang* [a], *Zhenghua Tang* [a,b,*], *Shaowei Chen* [c,**]

[a] *Guangzhou Key Laboratory for Surface Chemistry of Energy Materials and New Energy Research Institute, School of Environment and Energy, South China University of Technology, Guangzhou Higher Education Mega Centre, Guangzhou, 510006, PR China*

[b] *Guangdong Engineering and Technology Research Center for Surface Chemistry of Energy Materials, School of Environment and Energy, South China University of Technology, Guangzhou Higher Education Mega Centre, Guangzhou, 510006, PR China*

[c] *Department of Chemistry and Biochemistry, University of California, 1156 High Street, Santa Cruz, CA, 95064, United States*

HIGHLIGHTS

- A facile strategy was developed for fabricating high-performance Ru-based catalysts.
- Ru nanoparticles and Ru single atoms are encapsulated in the pores of NMCNs.
- Ru-NMCNs-500 had superior HER activity and long-term stability to Pt/C in 1 M KOH.
- It opens a new avenue for preparing HER catalysts under extreme alkaline conditions.

GRAPHICAL ABSTRACT

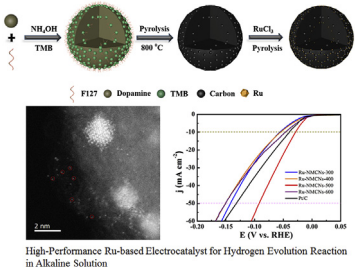

High-Performance Ru-based Electrocatalyst for Hydrogen Evolution Reaction in Alkaline Solution

ARTICLE INFO

Article history:
Received 7 January 2020
Received in revised form
7 April 2020
Accepted 7 May 2020
Available online 31 May 2020

ABSTRACT

Hydrogen evolution reaction (HER) plays a critical role in electrocatalysis, and developing highly active, cheap and stable Pt-free catalysts for HER in alkaline media is imperative for conversion of renewable energy into hydrogen fuels via photo/electrochemical water splitting. Herein, we report a facile strategy to fabricate a high-performance Ru-NMCNs-T electrocatalyst (T is the annealing temperature) for HER, which consist of both Ru nanoparticles and single Ru atoms well dispersed on nitrogen-doped mesoporous carbon nanospheres (NMCNs). Ru-NMCNs-500 exhibited the best HER performance in the series.

* *Corresponding author*. Guangzhou Key Laboratory for Surface Chemistry of Energy Materials and New Energy Research Institute, School of Environment and Energy, South China University of Technology, Guangzhou Higher Education Mega Centre, Guangzhou, 510006, PR China.

** *Corresponding author*.

E-mail addresses: zhht@scut.edu.cn (Z. Tang), shaowei@ucsc.edu (S. Chen).

https://doi.org/10.1016/j.ijhydene.2020.05.064

Keywords:
Hydrogen evolution reaction
Ru-based electrocatalysts
Nitrogen-doped mesoporous carbon nanospheres
Ru single atoms
Alkaline solution

To achieve a current density of 10 mA cm^{-2} in 1 M KOH, it only needs an overpotential of 28 mV with a small Tafel slope of 35.2 mA dec^{-1}, superior to the commercial Pt/C catalyst. It also exhibited exceedingly improved long-term stability than Pt/C. This study can open a new avenue for preparing Ru-based catalysts toward HER under extreme alkaline conditions.

Introduction

To combat the serious problems associated with fossil fuel-based energy sources, it is urgent to develop clean and renewable energy alternatives [1]. In this regard, hydrogen has been widely deemed as one of the most promising clean energies because of its high mass energy density (120 MJ kg^{-1}) and pollution-free nature [2–4]. The water electrolysis through the hydrogen evolution reaction (HER) is an important process for efficient energy conversion by generating hydrogen [5–8]. Photochemical synthesis can achieve hydrogen production, but there are some possible disadvantages, such as the solar energy is too scattered and not stable, not to mention that the preparations of solar cells are sophisticated and costly [9–12]. In contrast, electrochemical HER can be more efficient and reliable, the excess electricity can be fully utilized, and the produced hydrogen is extremely pure as well. However, the high overpotential for electrochemical water splitting makes the hydrogen production very difficult to proceed, hence a catalyst to trigger the proton reduction with minimal overpotential to enhance the HER kinetics is imperative [13,14]. Currently, Pt and Pt-based materials hold "The Holy Grail" for HER due to its near zero overpotential and excellent long-term durability. However, the acute scarcity and high cost of Pt significantly impede the large-scale commercialization [15,16]. Furthermore, electrochemical water splitting can be conducted in either acid or alkaline solution, where acidic electrolytes are commercially and technologically limited by a lack of cheap and efficient counter electrode catalysts in acid environment. To that end, a great deal of research efforts have been devoted to developing all kinds of HER catalysts which exhibit high activity and robust stability in alkaline media [17–25].

Ruthenium (Ru)-based nanomaterials have been emerged as promising alternative catalysts for HER because of the economic advantage of Ru (Ru is ~3-fold cheaper than Pt), excellent activity, and long-term performance stability of the catalysts [26,27]. To achieve desirable HER activity in alkaline media, developing effective means to optimize the size and morphology and increase the surface area of the Ru-based catalysts is highly desirable. For instance, Wang et al. reported a general solid-phase approach for the green and facile fabrication of highly dispersed uncapped Ru nanoparticles for HER, where the small size and uniform dispersion were accountable for the superior HER performance [28]. Qiao group reported an anomalously structured Ru catalyst that showed 2.5 times higher hydrogen generation rate than Pt, and the high activity probably originated from its suitable adsorption energies to some key reaction intermediates in the HER process [29]. To improve the sluggish HER rate in alkaline media, decreasing the high water-dissociation (Volmer step) energy barrier is highly desirable. To that end, introducing a support which can collectively enhance Volmer and Heyrovsky/Tafel step hence promoting the HER performance is a viable and effective strategy [30]. Nitrogen-doped carbon matrix would be an ideal choice as a support, as it not only can endow the catalyst high conductivity, but also can impart the uniform dispersion of the active sites, hence the active sites in the electrolyte can be well-protected and the catalyst could maintain a high durability in long-term operations [31–34]. Moreover, the doped electro-negative nitrogen atoms not only enhance the electrical conductivity of the substrate, but also improve the metal-substrate interaction hence promote the electrocatalytic performance [35]. By loading ruthenium nanoparticles into a novel carbon, the as-prepared catalyst reported by Li et al. exhibited excellent catalytic behavior with an overpotential of 0 mV, a Tafel slope of 47 mV dec^{-1}, and an outstanding durability in 1 M KOH [36]. Nanda group demonstrated the facile synthesis of ultrafine Ru nanocrystals supported by N-doped graphene as an exceptional HER catalyst in alkaline solution, where the electron transfer from Ru to carbon resulted in an electron-deficient metal center hence greatly enhanced the activity [37]. Ping and Chen groups prepared a catalyst of ruthenium atomically dispersed in porous carbon, of which the catalytic performance was markedly better than that of commercial platinum catalyst, with an overpotential of only −12 mV to reach the current density of 10 mV cm^{-2} in 1 M KOH and −47 mV in 0.1 M KOH [38]. In a recent study, Kweon et al. developed a simple synthetic route to prepare Ru nanoparticles uniformly anchored onto the surface of multiwalled carbon nanotubes (MWCNTs) [39]. Briefly, following the formation of ruthenium carboxylate complexes, the chemical and thermal annealing were able to turn Ru^{3+} ions into Ru(0) particles onto the surface of MWCNTs. Remarkably, in a practical water-splitting test, the Ru@MWCNTs catalyst exhibited an average Faradaic efficiency of 92.28% at 1.8 V, leading to 15.4% higher hydrogen production per power consumption than that of Pt/C [39].

Recently, single atom catalysts have been gaining tremendously increasing research attentions, thanks to their exceptional catalytic activities, maximal atomic utilizations, and strong metal-support interactions [40–42]. To enhance the catalytic performance and further lower the cost, it would be highly desirable that single Ru atoms can be incorporated into Ru-based catalysts. Herein, we report a facile approach to prepare a series of high-performance Ru-based electrocatalyst for HER in alkaline media, and the catalysts consist of both Ru

nanoparticles and single Ru atoms well dispersed on nitrogen-doped mesoporous carbon nanospheres (NMCNs). Among the Ru-NMCNs-T (T is the annealing temperature) series, the Ru-NMCNs-500 sample demonstrated the best HER activity in 1 M KOH, superior to the commercial Pt/C catalyst. It also showed higher long-term stability than Pt/C with great robustness.

Experimental section

Chemicals

Ruthenium (III) chloride hydrate ($RuCl_3 \cdot 3H_2O$, 99%), triblock poly (ethylene oxide)-*b*-poly (propylene oxide)-*b*-poly (ethylene oxide), pluronic F127 ($EO_{106}PO_{70}EO_{106}$, MW = 12,600), 1, 3, 5-trimethylbenzene (C_9H_{12}, TMB), ammonium hydroxide (NH_4OH, 28–30 wt%), Al_2O_3 powders and dopamine hydrochloride ($C_8H_{11}NO_2 \cdot HCl$) were purchased from Energy Chemicals (Shanghai, China). Commercial Pt/C (20 wt%) was obtained from Alfa Aesar (China). Ethanol was bought from Zhiyuan Chemical Industry (Tianjin, China). The water used in this study was ultrapure with a resistivity of 18.2 MΩ cm^{-1}. All the chemicals were directly used without further purification.

Preparation of nitrogen-doped mesoporous carbon nanospheres

The synthesis of nitrogen-doped mesoporous carbon nanospheres (denoted as NMCNs) was conducted by following the previously reported approach [43]. Typically, 1.0 g of F127 and 0.5 g of dopamine hydrochloride were first co-dissolved in a mixed solvent containing 50 mL of water and 50 mL of ethanol, then the mixture was kept stirring vigorously at room temperature to form a transparent solution. Subsequently, 2.0 mL of TMB was slowly injected into the solution under stirring for 30 min to form an emulsion. Then, 5.0 mL of ammonia was added dropwise at a rate of 30 mL h^{-1} into the above mixture to induce the self-polymerization of dopamine. The mesoporous TMB/F127/PDA polymer nanospheres were collected by centrifugation and then washed with water and ethanol 3–5 times. After preheating the mesoporous TMB/F127/PDA polymer nanospheres at 350 °C for 3 h then 800 °C for 2 h under N_2 atmosphere with a temperature increasing rate of 2 °C min^{-1}, the obtained solid was collected as the final product of NMCNs.

Preparation of the Ru-NMCNs-T samples

The Ru-NMCNs-T samples were prepared in a following manner. Firstly, the $RuCl_3 \cdot 3H_2O$ (0.1 g mL^{-1}) solution were added into the NMCNs aqueous dispersion (100 mg NMCNs dispersed in 50 mL of deionized water) and kept stirring at room temperature for 10 h. Then, the solid was collected by centrifugation and dried at 35 °C under vacuum overnight. The solid was heated at a controlled temperature (300, 400, 500, and 600 °C) for 2 h at a heating rate of 5 °C min^{-1} under H_2/Ar (5%/95%) atmosphere, and collected as the final product. The samples were denoted as Ru-NMCNs-T (T is the annealing temperature, i.e. 300 °C, 400 °C, 500 °C, or 600 °C).

Characterizations

Field-emission scanning electron microscopy (FE-SEM, Merlin) and transmission electron microscopy (TEM, JEM-2100F) equipped with energy-dispersive X-ray spectroscopy (EDS) were used to observe the surface morphology and microscopic structure of the samples. The elemental mapping of the Ru-NMCNs-500 was acquired on the above TEM instrument. High angle annular dark field imaging scanning transmission electron microscopy (HAADF-STEM) was performed using a JEM-ARM300F machine operated at 300 kV. X-ray diffraction (XRD) patterns were recorded on a Bruker D8 diffractometer with a scan range from 10° to 90° at 2° min^{-1} (Cu K_α radiation, λ = 0.1541 nm). X-ray photoelectron spectroscopic (XPS) measurements were performed on a Phi X-tool instrument using Al as the exciting source. Raman spectra were obtained using a Raman spectrometer (Renishaw, Inc, RM-2000) with a 532 nm laser source. The BET surface area and pore size were measured on a Quantachrome Autosorb-iQ instrument with nitrogen adsorption at 77 K using the density functional theory method.

Electrochemical measurements

Electrochemical measurements were carried out with a conventional three-electrode configuration on a CHI 750E electrochemical workstation (CHI Instruments, China). A graphite rod and an Ag/AgCl (3 M KCl) electrode were employed as the counter electrode and reference electrode, respectively. The catalyst ink was prepared as follows: 2.5 mg of the catalyst (i.e., Ru-NMCNs or 20 wt% Pt/C) was first dispersed in a mixture of ethanol (0.4 mL) and Nafion (0.5 wt%, 100 μL) under ultrasonication for 30 min. Then, 5.0 μL of the above suspension (corresponding to a loading amount of 0.357 mg cm^{-2}) was dropwisely cast onto the polished glassy carbon electrode (GCE, surface area of 0.07 cm^2) and dried naturally at room temperature. The GCE was polished with Al_2O_3 powders, and the electrochemical measurement was performed in 1 M KOH solution. Linear sweep voltammetric (LSV) measurement was conducted between −0.7 and −1.5 V with a scan rate of 10 mV s^{-1}, the potential measured against Ag/AgCl was converted into potential versus reversible hydrogen electrode (RHE) according to the equation, E (vs. RHE) = E (vs. Ag/AgCl) + 0.197 V + 0.059 * pH. CV test was conducted from −1.2 V to −0.9 V at a sweep rate of 100 mV s^{-1} for 10, 000 cycles to investigate the cycling stability.

To determine the electrochemically active surface area (EASA) of the samples, a series of CV curves were recorded at various scan rates (5, 10, 15, 20, 30 mV s^{-1}) in non-Faradic region (72–212 mV vs. RHE in 1 M KOH). Then, a typical specific capacitance (EASA = C_{dl}/C_S, the Cs value of 0.035 mF cm^{-2} in alkaline solutions was used based on the reported average Cs of metallic surfaces, the C_{dl} value is the slope obtained from the resulted straight line) was employed to calculate the EASA value [26,44].

Results and discussion

TEM and SEM analysis

Fig. 1 shows the schematic for preparing the Ru-NMCNs-T samples. It includes roughly three steps (See details in experimental section) [43]. As presented in Fig. 1, F127 reacting with dopamine in the presence of TMB in NH_4OH can form mesoporous TMB/F127/PDA polymer nanospheres, which are subjected to pyrolysis at 800 °C to generate nitrogen-doped mesoporous carbon nanospheres (NMCNs). Lastly, $RuCl_3 \cdot 3H_2O$ was added into the NMCNs dispersion and the mixture was annealed under a H_2/Ar atmosphere. The obtained solid was then collected as the final product and denoted as Ru-NMCNs-T, where T denotes the annealing temperature.

The morphological change during the preparation process of Ru-NMCNs-T was monitored by electronic microscopy. As illustrated in Fig. 2a, field-emission scanning electron microscopy (FESEM) images show that the polymerized TMB/F127/PDA nanospheres exhibited perfect-defined spherical shape with a good uniformity, and the average size of the nanoparticles can be estimated as 160 ± 20 nm. Such well-defined morphology of the spheres can be intact preserved into the final product of Ru-NMCNs, as evidenced by the FESEM image of Ru-NMCNs-500 in Fig. 2b. However, the particle size slightly decreased to 130 ± 12 nm, probably due to the thermal induced shrinkage. The transmission electron microscopic (TEM) images in Fig. 2c and d demonstrate that Ru nanoparticles are uniformly distributed onto the mesoporous carbon nanospheres, where the inset size distribution histogram depicts that the average size of Ru nanoparticles is 2.62 ± 0.49 nm. In addition, the corresponding nitrogen adsorption-desorption isotherms of NMCNs and Ru-NMCNs-500 can be found in Fig. S1. The surface area of Ru-NMCNs-500 is ~684 $m^2 g^{-1}$, and the pore size distribution based on the DFT model (inset in Fig. S1) is centered at ~3.79 nm, both are slightly lower than that of NMCNs (~755 $m^2 g^{-1}$ and ~4.22 nm), suggesting that the well-defined mesoporous structure of NMCNs was well-preserved upon the introduction of Ru and the Ru nanoparticles can be uniformly dispersed in the pores. High resolution TEM (HR-TEM) image (Fig. 2e) shows clearly identifiable lattice fringes with spacings of 0.234 and 0.205 nm, corresponding to the (100) and (101) planes of hcp Ru (JCPDS 06–0663), respectively [24,45]. The energy dispersive X-ray (EDX) elemental mapping images in Fig. 2f further demonstrate the uniform distribution of the C, N, and Ru elements. Furthermore, aberration corrected high-angle annular dark field STEM (HAADF-STEM) images (Fig. 2g and h) illustrate that there are not only Ru nanoparticles, but also a small amount of isolated Ru atoms (highlighted by red circles in Fig. 2i) can be readily identified on the NMCNs matrix. It is worth mentioning that, previous study has indicated that in the presence of both Ru nanoparticles and Ru single atoms, the single Ru atoms rather than Ru nanoparticles embedded within the carbon matrix contributed more to the performance of the HER activity in alkaline media [38]. Despite the low content, the individual Ru atoms in Ru-NMCNs-500 are probably beneficial for the HER performance. The elemental analysis (Fig. S2) shows that the total Ru content is 3.04 wt %, and in such low Ru ratio, single atoms of Ru are expected to be formed.

XRD and XPS measurements

The crystal phases of the Ru-NMCNs-T samples were then probed by the X-ray diffraction (XRD) test. As shown in Fig. 3a, there are two broad peaks at ~25° and ~44°, corresponding to the (002) and (100) plane of the disordered carbonaceous structure, respectively. The Raman spectra of NMCNs and Ru-NMCNs-500 are illustrated in Fig. S3, where two obvious peaks around 1350 and 1590 cm^{-1} in both samples can be attributed to the disordered carbon (D band) and ordered graphitic carbon (G band), respectively [43]. Notably, the intensity ratio (I_D/I_G) for Ru-NMCNs-500 (~1.03) is slightly larger than that of NMCNs (~1), indicating an increase of structural defects upon the introduction of the Ru species. It has been documented that such defects are favorable for improving the catalytic performance [46,47]. Meanwhile, the other peaks with 2θ positioned at ~38°, ~42°, ~44°, ~58°, ~69° and ~78° can be indexed to (100), (002), (101), (102), (110), and (103) facets of crystalline Ru (JCPDS 06–0663). One may notice that, with the increasing of the annealing temperature, the peak intensity in XRD enhanced, suggesting that higher temperature is favorable for forming crystalline Ru. Additionally, the XRD patterns of the Ru-NMCNs-500 sample with different initial Ru loadings were studied (Fig. S4), and higher Ru content in the sample tend to display higher peak intensities, as expected.

The chemical composition and electronic configuration of the samples were then investigated by X-ray photoelectron spectroscopy (XPS). As depicted in Fig. S5, the presence of C, N, O, and Ru elements in Ru-NMCNs-500 is confirmed. The

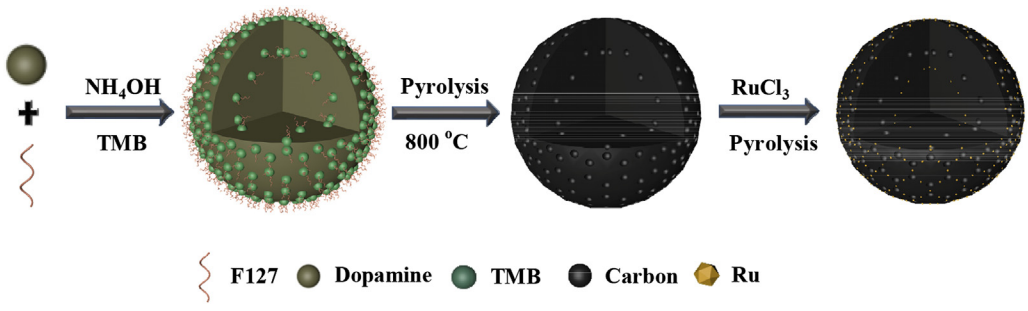

Fig. 1 – Schematic for preparing the Ru-NMCNs-T samples (T is the annealing temperature).

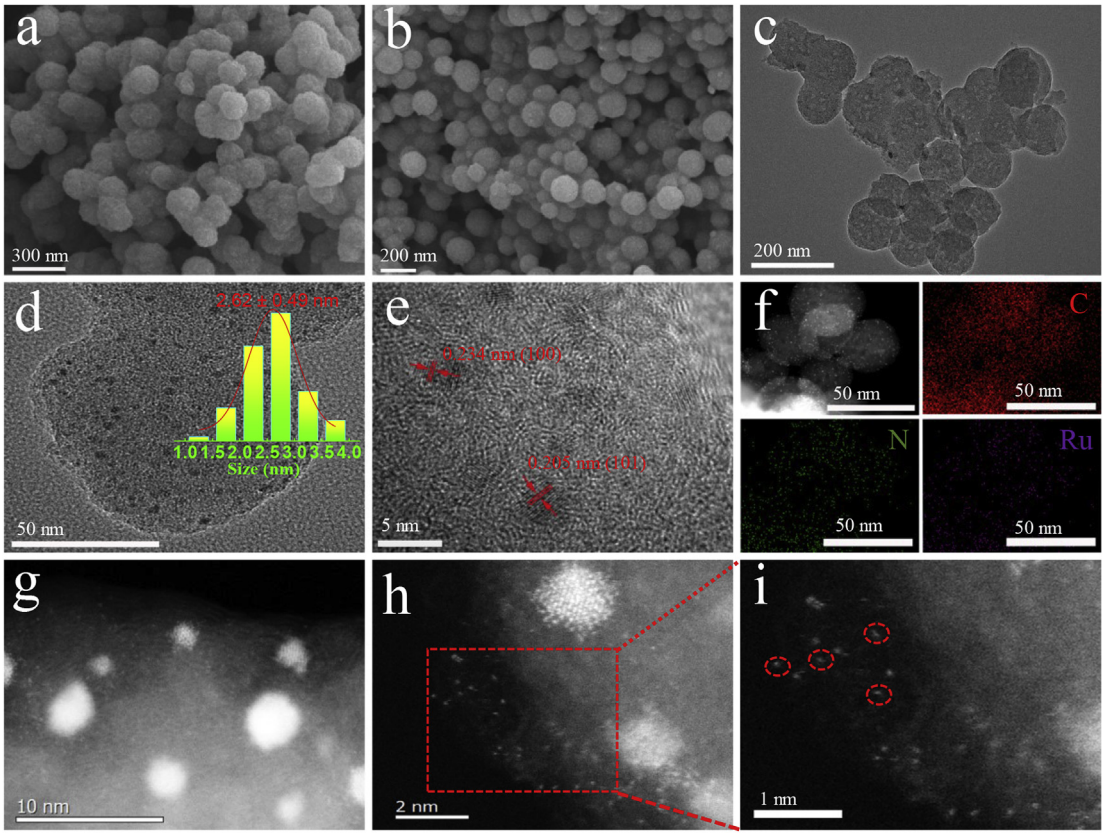

Fig. 2 – Representative FESEM images of the TMB/F127/PDA nanospheres (a) and Ru-NMCNs-500 (b), TEM images of Ru-NMCNs-500 at different magnifications (c–e). Inset: particle size distribution histogram. Scale bars are (c) 200 nm, (d) 50 nm, and (e) 5 nm. TEM-EDX mapping images of Ru-NMCNs-500 (f) for the C, N, and Ru elements. HAADF-STEM images of Ru-NMCNs-500 (g–h), and magnified HAADF-STEM image (i).

atomic percentages of the C, N, and Ru atoms estimated from XPS are summarized in Table S1. It can be noted that, C atoms dominated the sample, while the N and Ru atoms had a 4.25% and 5.57% weight ratio, respectively. Note that, the weight percentages of the N and Ru atoms from XPS are slightly larger than that from EDS, this is probably due to that XPS is a surface detection technique with the detection depth of only a few nanometers while the N and Ru atoms are more prone to be enriched on the surface of NMCNs. The core-level XPS spectra of the N1s electron from NMCNs and Ru-NMCNs-500 are illustrated in Fig. 3b. For both samples, the broad peak can be deconvoluted into four subpeaks, which are assigned to pyridinic N (398.2 eV), pyrrolic N (399.8 eV), graphitic N (400.9 eV), and oxidized N (402.5 eV), respectively [38,43,48]. Based on the integrated peak area, the content of four different N species for NMCNs and Ru-NMCNs-500 can be estimated and summarized in Table S2. One may notice that, compared with NMCNs, the contents of the pyridinic N, pyrrolic N and graphitic N all decreased in Ru-NMCNs-500, while the content of oxidized N significantly increased, suggesting that Ru atoms are probably coordinated with the three N species rather than oxidized N species.

Fig. 3c presents the high resolution XPS spectra of the Ru3p electrons, where the two peaks with binding energies at 485.0 and 462.6 eV can be assigned to the $Ru3p_{1/2}$ and $Ru3p_{3/2}$ electrons from metallic Ru, respectively [49,50]. It suggests Ru atoms in the precursor have been fully reduced, and they exist as Ru (0) in the sample. Lastly, the spectra from the C1s plus Ru3d electrons is shown in Fig. 3d. The C1s peak suggest there are two types of carbon species consisting of C=C (284.4 eV) and C=N (285.5 eV) [51,52]. Moreover, the small peak adjacent with the binding energy at 284.4 eV can be attributed from the $Ru3d_{5/2}$ electrons of the metallic Ru, further attest the exclusive presence of metallic Ru in the sample.

The HER performance of the series and Pt/C in 1 M KOH

The HER electrocatalytic activities of the Ru-NMCNs-T samples were then systematically studied in 1.0 M KOH using a standard three-electrode system and compared with the commercial Pt/C catalyst. The polarization curves in 1 M KOH are illustrated in Fig. 4a, where all the catalysts exhibited almost zero onset potential. However, to afford the current density of 10 mA cm^{-2}, the overpotential was 55, 54, 28, and 46 mV for Ru-NMCNs-300, Ru-NMCNs-400, Ru-NMCNs-500, and Ru-NMCNs-600, respectively. It can be noted that, with the increasing of thermal annealing temperature, the HER activity first increased then diminished. Ru-NMCNs-500 exhibited the best HER activity, of which the overpotential even smaller than that of Pt/C (39 mV) at 10 mA cm^{-2}. Such trend is more apparent at higher current density (e. g.

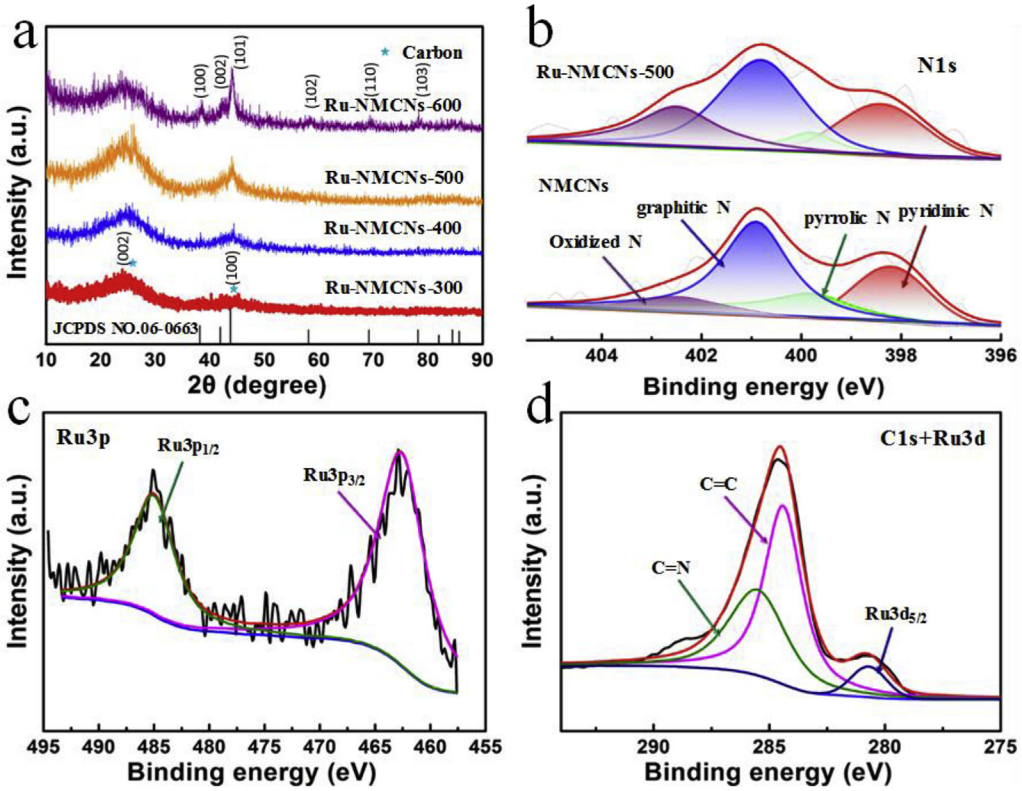

Fig. 3 – The XRD patterns of the Ru-NMCNs-T samples (a). The core-level XPS spectra of the N1s electrons for NMCNs and Ru-NMCNs-500 (b), The core-level XPS spectra of the Ru3p electrons (c), and the C1s + Ru3d electrons (d) from Ru-NMCNs-500.

50 mA cm^{-2}), confirming that 500 °C is the optimal annealing temperature. In addition, with the 500 °C annealing temperature, the samples of different initial Ru mass loadings were also investigated for HER in 1 M KOH (Fig. S6), where the 10% mass loading exhibited the best activity. The Tafel plots of the Ru-NMCNs-T series are displayed in Fig. 4b, and the Tafel slopes can be extracted. The Tafel slope for Ru-NMCNs-500 is 35.2 mV dec^{-1}, smaller than that of Pt/C (41 mV dec^{-1}), Ru-NMCNs-300 (57.6 mV dec^{-1}), Ru-NMCNs-400 (64.8 mV dec^{-1}), and Ru-NMCNs-600 (59.8 mV dec^{-1}), indicating that Ru-NMCNs-500 has a much faster HER kinetics. Specifically, the HER process in alkaline solution can be described as three steps [27,53]:

Volmer reaction: $H_2O + e^- + M \rightarrow M-H + OH^-$

Heyrovsky reaction: $M-H + H_2O + e^- \rightarrow H_2 + OH^- + M$

Tafel reaction: $M-H + M-H \rightarrow 2M + H_2$

As the Tafel slope of Ru-NMCNs-500 is close to that of Pt/C, it indicates that a Tafel-Volmer mechanism is probably adopted [54].

The electrochemical impedance spectroscopy of the samples was then conducted [27,55]. The Nyquist plots are illustrated in Fig. 4c, where Ru-NMCNs-600 exhibited the largest semicircle and Ru-NMCNs-500 exhibited the smallest semicircle as anticipated. Inset shows the fitted Nyquist plots through the well-known Randles equivalent circuit to calculate the resistance (Rs) and charge transfer resistance (Rct) of the catalyst [29], and the fitted results are compiled in Table S3. Ru-NMCNs-500 had the smallest Rct value of 8.86 Ω in the series, lower than that of Pt/C (9.22 Ω) as well. The trend of the Rct value agrees well with the HER activity. To further unravel the physical origin for the HER activity difference between Ru-NMCNs-500 and Pt/C, the electrochemically active surface area (EASA) test was performed. As shown in Fig. S7, the calculated EASA value of Ru-NMCNs-500 is 270.28 cm^2, about 2-fold larger than that of Pt/C (94.285 cm^2).

It is worth noting that, the HER performance of the as-prepared Ru-NMCNs-500 sample is at least comparable, if not superior, with recently documented Ru-based top-level electrocatalysts in 1 M KOH, and the comparison results are summarized in Table S4. For instance, to afford a current density of 10 mA cm^{-2}, the required overpotential for Ru-NMCNs-500 is 28 mV, much smaller than that of Ru/g-C_3N_4/C (79 mV) [29], Ru/C (53 mV) [24], RuP_2@NPC (52 mV) [56], Ru–Ru_2P@PC (43 mV) [57], RuP@NPC (74 mV) [31], Ru/C–TiO_2 (44 mV) [30], and RuP_2/CNTs (40 mV) [58], and also comparable with that of Ru@NC (26 mV) [59], Ru@CN (32 mV) [60], RuCo@NC (28 mV) [61], Ru–MoO_2 (29 mV) [62], Ni@Ni_2P–Ru HNRs (31 mV) [63], NiRu@N–C (32 mV) [64], Pd–Ru@NG (28 mV) [65], and Ru_xP@NPC/GHSs (25.5 mV) [66].

Moreover, the long-term stability is another critical criterion to assess the performance of the catalyst for HER. The polarization curves were then acquired for Ru-NMCNs-500

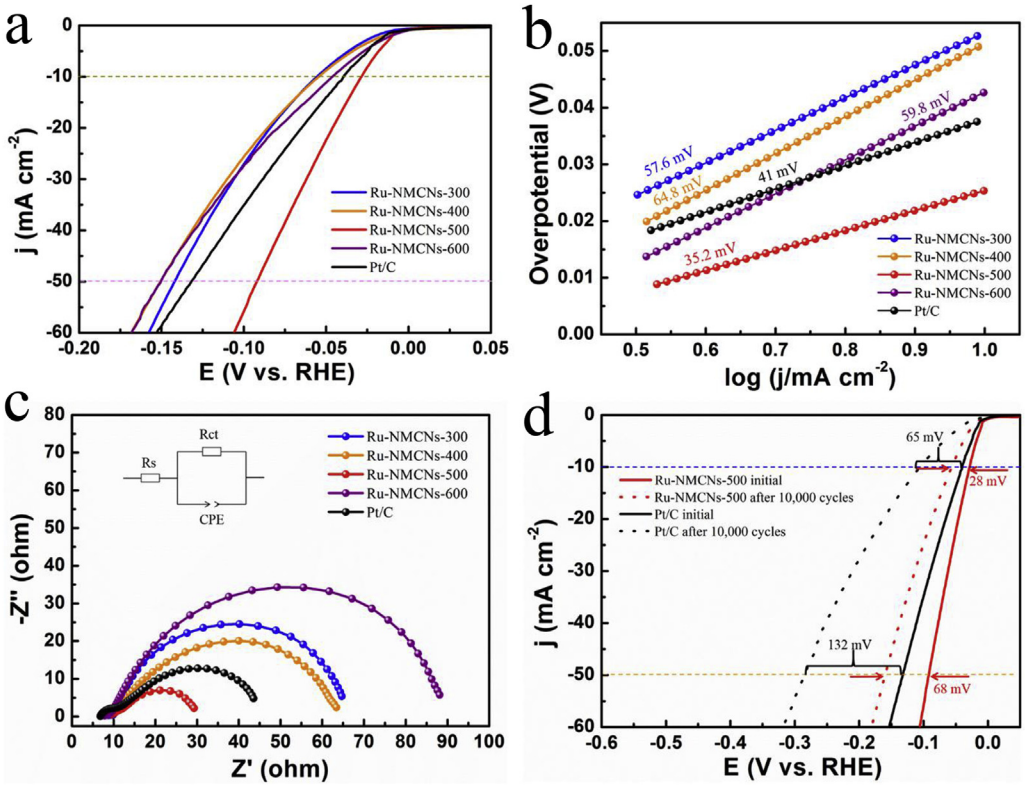

Fig. 4 – Polarization curves of Ru-NMCNs-T and Pt/C in 1 M KOH (a), and the corresponding Tafel plots (b). Nyquist plots collected at the overpotential of −10 mV (vs RHE) (c). Initial and the 10 000th polarization curves of Ru-NMCNs-500 and Pt/C recorded in 1 M KOH (d).

and Pt/C before and after 10 000 cycles of potential scans. As presented in Fig. 4d, after 10 000 cycles, at 10 mA cm^{-2}, the overpotential shifted negatively 28 mV for Ru-NMCNs-500, while at 50 mA cm^{-2}, the overpotential shifted negatively 68 mV for Ru-NMCNs-500, both are much smaller than that of Pt/C (65 mV at 10 mA cm^{-2} and 152 mV at 50 mA cm^{-2}). It indicates the remarkably superior long-term stability of Ru-NMCNs-500 outperforming Pt/C. Intriguingly, TEM images of the recycled Ru-NMCNs-500 sample also reveals that there is no obvious morphological change after the stability test (Fig. S8). The findings confirm that Ru-NMCNs-500 is a stable and excellent electrocatalyst under extreme alkaline conditions.

There are several reasons that account for the outstanding performance of the Ru-NMCNs-500 sample. First of all, the nitrogen-doped mesoporous carbon nanospheres not only increase the electric conductivity of the composite, but also provide abundant well-defined pores for electron transfer and mass transport during the electrocatalytic process [34,67]; Secondly, there are not only Ru nanoparticles, but also single Ru atoms, and previous investigation has demonstrated that the single Ru atoms with coordinated nitrogen and carbon sites can make a great contribution to boost the HER activity [38]. Finally, the Ru nanoparticles and isolated Ru atoms are well encapsulated in the pores and cavities of the NMCNs, which can prevent the Ru species from aggregation, leaching, and coalescence, hence drastically promoted the long-term stability for HER [68,69].

Conclusions

In summary, we report a facile approach to fabricate the Ru-NMCNs-T catalysts consisting of both Ru nanoparticles and single Ru atoms embedded in nitrogen-doped mesoporous carbon nanospheres for HER in 1 M KOH. The Ru-NMCNs-500 sample exhibited the best HER activity in the series, superior to the Pt/C catalyst. It also demonstrated markedly higher long-term stability than Pt/C. The intriguing HER properties of Ru-NMCNs-500 can be attributed the merits of NMCNs, the synergistic catalytic effects between Ru and NMCNs, as well as the presence of the single Ru atoms. This study can shed light on preparing cheap, high performance and durable Ru-based electrocatalyst for HER in extreme alkaline solution and beyond. We envision that more research efforts will be devoted to engineering single atom dominated Ru-based catalysts for producing high-purity hydrogen in both fundamental and practical aspects.

Acknowledgements

Z. T. acknowledges financial support from Guangdong Natural Science Funds for Distinguished Young Scholars (No. 2015A030306006), Guangzhou Science and Technology Plan Projects (No. 201804010323), and the fundamental funds for central universities (SCUT No. 2018ZD022). S. C. thanks the

National Science Foundation for partial support of the work (CHE-1710408 and CBET-1848841).

Appendix ASupplementary data

Supplementary data to this article can be found online at https://doi.org/10.1016/j.ijhydene.2020.05.064.

REFERENCES

[1] Chu S, Majumdar A. Opportunities and challenges for a sustainable energy future. Nature 2012;488:294–303.
[2] Turner JA. Sustainable hydrogen production. Science 2004;305:972.
[3] Saeedmanesh A, Kinnon MM, Brouwer J. Hydrogen is essential for sustainability. Curr Opin Electrochem 2018;12:166–81.
[4] Zinatloo-Ajabshir S, Salehi Z, Amiri O, Salavati-Niasari M. Green synthesis, characterization and investigation of the electrochemical hydrogen storage properties of $Dy_2Ce_2O_7$ nanostructures with fig extract. Int J Hydrogen Energy 2019;44:20110–20.
[5] Karunadasa HI, Chang CJ, Long JR. A molecular molybdenum-oxo catalyst for generating hydrogen from water. Nature 2010;464:1329–33.
[6] Strmcnik D, Lopes PP, Genorio B, Stamenkovic VR, Markovic NM. Design principles for hydrogen evolution reaction catalyst materials. Nanomater Energy 2016;29:29–36.
[7] Li Y, Yin J, An L, Lu M, Sun K, Zhao Y-Q, Gao D, Cheng F, Xi P. FeS_2/CoS_2 interface nanosheets as efficient bifunctional electrocatalyst for overall water splitting. Small 2018;14:1801070.
[8] Deng S, Zhang K, Xie D, Zhang Y, Zhang Y, Wang Y, Wu J, Wang X, Fan HJ, Xia X, Tu J. High-index-faceted Ni_3S_2 branch arrays as bifunctional electrocatalysts for efficient water splitting. Nano-Micro Lett 2019;11:12.
[9] Park HG, Holt JK. Recent advances in nanoelectrode architecture for photochemical hydrogen production. Energy Environ Sci 2010;3:1028–36.
[10] Sabet M, Salavati-Niasari M, Amiri O. Using different chemical methods for deposition of CdS on TiO_2 surface and investigation of their influences on the dye-sensitized solar cell performance. Electrochim Acta 2014;117:504–20.
[11] Mousavi-Kamazani M, Zarghami Z, Salavati-Niasari M. Facile and novel chemical synthesis, characterization, and formation mechanism of copper sulfide (Cu_2S, Cu_2S/CuS, CuS) nanostructures for increasing the efficiency of solar cells. J Phys Chem C 2016;120:2096–108.
[12] Rahman MZ, Kibria MG, Mullins CB. Metal-free photocatalysts for hydrogen evolution. Chem Soc Rev 2020;49:1887–931.
[13] Eftekhari A. Electrocatalysts for hydrogen evolution reaction. Int J Hydrogen Energy 2017;42:11053–77.
[14] Hossain A, Sakthipandi K, Atique Ullah AKM, Roy S. Recent progress and approaches on carbon-free energy from water splitting. Nano-Micro Lett 2019;11:103.
[15] Wang J, Zhang H, Wang X. Recent methods for the synthesis of noble-metal-free hydrogen-evolution electrocatalysts: from nanoscale to sub-nanoscale. Small Methods 2017;1:1700118.
[16] Wang J, Xu F, Jin H, Chen Y, Wang Y. Non-Noble metal-based carbon composites in hydrogen evolution reaction: fundamentals to applications. Adv Mater 2017;29:1605838.
[17] Zheng Z, Li N, Wang C-Q, Li D-Y, Zhu Y-M, Wu G. Ni–CeO_2 composite cathode material for hydrogen evolution reaction in alkaline electrolyte. Int J Hydrogen Energy 2012;37:13921–32.
[18] Liu T, Liu D, Qu F, Wang D, Zhang L, Ge R, Hao S, Ma Y, Du G, Asiri AM, Chen L, Sun X. Enhanced electrocatalysis for energy-efficient hydrogen production over CoP catalyst with nonelectroactive Zn as a promoter. Adv Energy Mater 2017;7:1700020.
[19] Wang W, Yang L, Qu F, Liu Z, Du G, Asiri AM, Yao Y, Chen L, Sun X. A self-supported $NiMoS_4$ nanoarray as an efficient 3D cathode for the alkaline hydrogen evolution reaction. J Mater Chem A 2017;5:16585–9.
[20] Zhang Y, Liu Y, Ma M, Ren X, Liu Z, Du G, Asiri AM, Sun X. A Mn-doped Ni_2P nanosheet array: an efficient and durable hydrogen evolution reaction electrocatalyst in alkaline media. Chem Commun 2017;53:11048–51.
[21] Dou S, Wang X, Wang S. Rational design of transition metal-based materials for highly efficient electrocatalysis. Small Methods 2018:1800211. 0.
[22] Wei J, Zhou M, Long A, Xue Y, Liao H, Wei C, Xu JZ. Heterostructured electrocatalysts for hydrogen evolution reaction under alkaline conditions. Nano-Micro Lett 2018;10:75.
[23] Zhang L, Ren X, Guo X, Liu Z, Asiri AM, Li B, Chen L, Sun X. Efficient hydrogen evolution electrocatalysis at alkaline pH by interface engineering of Ni_2P–CeO_2. Inorg Chem 2018;57:548–52.
[24] Li Y, Abbott J, Sun Y, Sun J, Du Y, Han X, Wu G, Xu P. Ru nanoassembly catalysts for hydrogen evolution and oxidation reactions in electrolytes at various pH values. Appl Catal B Environ 2019;258:117952.
[25] Li L, Qin Z, Ries L, Hong S, Michel T, Yang J, Salameh C, Bechelany M, Miele P, Kaplan D, Chhowalla M, Voiry D. Role of sulfur vacancies and undercoordinated Mo regions in MoS_2 nanosheets toward the evolution of hydrogen. ACS Nano 2019;13:6824–34.
[26] Tiwari JN, Harzandi AM, Ha M, Sultan S, Myung CW, Park HJ, Kim DY, Thangavel P, Singh AN, Sharma P, Chandrasekaran SS, Salehnia F, Jang J-W, Shin HS, Lee Z, Kim KS. High-performance hydrogen evolution by Ru single atoms and nitrided-Ru nanoparticles implanted on N-doped graphitic sheet. Adv Energy Mater 2019;9:1900931.
[27] Wu W, Wu Y, Zheng D, Wang K, Tang Z. Ni@Ru core-shell nanoparticles on flower-like carbon nanosheets for hydrogen evolution reaction at All-pH values, oxygen evolution reaction and overall water splitting in alkaline solution. Electrochim Acta 2019;320:134568.
[28] Wang Q, Ming M, Niu S, Zhang Y, Fan G, Hu J-S. Scalable solid-state synthesis of highly dispersed uncapped metal (Rh, Ru, Ir) nanoparticles for efficient hydrogen evolution. Adv Energy Mater 2018;8:1801698.
[29] Zheng Y, Jiao Y, Zhu Y, Li LH, Han Y, Chen Y, Jaroniec M, Qiao S-Z. High electrocatalytic hydrogen evolution activity of an anomalous ruthenium catalyst. J Am Chem Soc 2016;138:16174–81.
[30] Wang Y, Zhu Q, Xie T, Peng Y, Liu S, Wang J. Promoted alkaline hydrogen evolution reaction performance of Ru/C by introducing TiO_2 nanoparticles. ChemElectroChem 2020;7:1182–6.
[31] Chi J-Q, Gao W-K, Lin J-H, Dong B, Yan K-L, Qin J-F, Liu B, Chai Y-M, Liu C-G. Hydrogen evolution activity of ruthenium phosphides encapsulated in nitrogen- and phosphorous-codoped hollow carbon nanospheres. ChemSusChem 2018;11:743–52.
[32] Wang L, Tang Z, Yan W, Yang H, Wang Q, Chen S. Porous carbon-supported gold nanoparticles for oxygen reduction reaction: effects of nanoparticle size. ACS Appl Mater Interfaces 2016;8:20635–41.

[33] Wang Q, Wang L, Tang Z, Wang F, Yan W, Yang H, Zhou W, Li L, Kang X, Chen S. Oxygen reduction catalyzed by gold nanoclusters supported on carbon nanosheets. Nanoscale 2016;8:6629–35.
[34] Wang L, Tang Z, Yan W, Wang Q, Yang H, Chen S. Co@Pt Core@Shell nanoparticles encapsulated in porous carbon derived from zeolitic imidazolate framework 67 for oxygen electroreduction in alkaline media. J Power Sources 2017;343:458–66.
[35] Inagaki M, Toyoda M, Soneda Y, Morishita T. Nitrogen-doped carbon materials. Carbon 2018;132:104–40.
[36] Li W, Liu Y, Wu M, Feng X, Redfern SAT, Shang Y, Yong X, Feng T, Wu K, Liu Z, Li B, Chen Z, Tse JS, Lu S, Yang B. Carbon-quantum-dots-loaded ruthenium nanoparticles as an efficient electrocatalyst for hydrogen production in alkaline media. Adv Mater 2018;30:1800676.
[37] Barman BK, Das D, Nanda KK. Facile synthesis of ultrafine Ru nanocrystal supported N-doped graphene as an exceptional hydrogen evolution electrocatalyst in both alkaline and acidic media. Sustain Energy Fuels 2017;1:1028–33.
[38] Lu B, Guo L, Wu F, Peng Y, Lu JE, Smart TJ, Wang N, Finfrock YZ, Morris D, Zhang P, Li N, Gao P, Ping Y, Chen S. Ruthenium atomically dispersed in carbon outperforms platinum toward hydrogen evolution in alkaline media. Nat Commun 2019;10:631.
[39] Kweon DH, Okyay MS, Kim S-J, Jeon J-P, Noh H-J, Park N, Mahmood J, Baek J-B. Ruthenium anchored on carbon nanotube electrocatalyst for hydrogen production with enhanced Faradaic efficiency. Nat Commun 2020;11:1278.
[40] Zhu C, Shi Q, Feng S, Du D, Lin Y. Single-atom catalysts for electrochemical water splitting. ACS Energy Lett 2018;3:1713–21.
[41] Wang A, Li J, Zhang T. Heterogeneous single-atom catalysis. Nat Rev Chem 2018;2:65–81.
[42] Ji S, Chen Y, Wang X, Zhang Z, Wang D, Li Y. Chemical synthesis of single atomic site catalysts. Chem Rev 2020. https://doi.org/10.1021/acs.chemrev.9b00818.
[43] Peng L, Hung C-T, Wang S, Zhang X, Zhu X, Zhao Z, Wang C, Tang Y, Li W, Zhao D. Versatile nanoemulsion assembly approach to synthesize functional mesoporous carbon nanospheres with tunable pore sizes and architectures. J Am Chem Soc 2019;141:7073–80.
[44] Sun W, Cao L-m, Yang J. Conversion of inert cryptomelane-type manganese oxide into a highly efficient oxygen evolution catalyst via limited Ir doping. J Mater Chem A 2016;4:12561–70.
[45] Li F, Han G-F, Noh H-J, Ahmad I, Jeon I-Y, Baek J-B. Mechanochemically assisted synthesis of a Ru catalyst for hydrogen evolution with performance superior to Pt in both acidic and alkaline media. Adv Mater 2018;30:1803676.
[46] Dai Y, Jiang H, Hu Y, Fu Y, Li C. Controlled synthesis of ultrathin hollow mesoporous carbon nanospheres for supercapacitor applications. Ind Eng Chem Res 2014;53:3125–30.
[47] Lu Q, Wang A-L, Gong Y, Hao W, Cheng H, Chen J, Li B, Yang N, Niu W, Wang J, Yu Y, Zhang X, Chen Y, Fan Z, Wu X-J, Chen J, Luo J, Li S, Gu L, Zhang H. Crystal phase-based epitaxial growth of hybrid noble metal nanostructures on 4H/fcc Au nanowires. Nat Chem 2018;10:456–61.
[48] Zhang J, Qu L, Shi G, Liu J, Chen J, Dai LN. P-codoped carbon networks as efficient metal-free bifunctional catalysts for oxygen reduction and hydrogen evolution reactions. Angew Chem Int Ed 2016;55:2230–4.
[49] Sun S-W, Wang G-F, Zhou Y, Wang F-B, Xia X-H. High-performance Ru@C4N electrocatalyst for hydrogen evolution reaction in both acidic and alkaline solutions. ACS Appl Mater Interfaces 2019;11:19176–82.
[50] Zhang H, Ma Z, Duan J, Liu H, Liu G, Wang T, Chang K, Li M, Shi L, Meng X, Wu K, Ye J. Active sites implanted carbon cages in core–shell architecture: highly active and durable electrocatalyst for hydrogen evolution reaction. ACS Nano 2016;10:684–94.
[51] Niu W, Li L, Liu X, Wang N, Liu J, Zhou W, Tang Z, Chen S. Mesoporous N-doped carbons prepared with thermally removable nanoparticle templates: an efficient electrocatalyst for oxygen reduction reaction. J Am Chem Soc 2015;137:5555–62.
[52] Wang N, Lu B, Li L, Niu W, Tang Z, Kang X, Chen S. Graphitic nitrogen is responsible for oxygen electroreduction on nitrogen-doped carbons in alkaline electrolytes: insights from activity attenuation studies and theoretical calculations. ACS Catal 2018;8:6827–36.
[53] Zhong C, Zhou Q, Li S, Cao L, Li J, Shen Z, Ma H, Liu J, Zhang H, Lu M-H. Enhanced synergistic catalysis by novel triple-phase interfaces design of NiO/Ru@Ni for hydrogen evolution reaction. J Mater Chem A 2019;7:2344–50.
[54] Ding Z, Tang Z, Li L, Wang K, Wu W, Chen X, Wu X, Chen S. Ternary PtVCo dendrites for the hydrogen evolution reaction, oxygen evolution reaction, overall water splitting and rechargeable Zn–air batteries. Inorg Chem Front 2018;5:2425–31.
[55] Qian Z, Chen Y, Tang Z, Liu Z, Wang X, Tian Y, Gao W. Hollow nanocages of NixCo1−xSe for efficient zinc–air batteries and overall water splitting. Nano-Micro Lett 2019;11:28.
[56] Pu Z, Amiinu IS, Kou Z, Li W, Mu S. RuP2-Based catalysts with platinum-like activity and higher durability for the hydrogen evolution reaction at all pH Values. Angew Chem Int Ed 2017;56:11559–64.
[57] Liu Z, Li Z, Li J, Xiong J, Zhou S, Liang J, Cai W, Wang C, Yang Z, Cheng H. Engineering of Ru/Ru2P interfaces superior to Pt active sites for catalysis of the alkaline hydrogen evolution reaction. J Mater Chem A 2019;7:5621–5.
[58] Cheng M, Geng H, Yang Y, Zhang Y, Li CC. Optimization of the hydrogen-adsorption free energy of Ru-based catalysts towards high-efficiency hydrogen evolution reaction at all pH. Chem Eur J 2019;25:8579–84.
[59] Wang Z-L, Sun K, Henzie J, Hao X, Li C, Takei T, Kang Y-M, Yamauchi Y. Spatially confined assembly of monodisperse ruthenium nanoclusters in a hierarchically ordered carbon electrode for efficient hydrogen evolution. Angew Chem Int Ed 2018;57:5848–52.
[60] Wang J, Wei Z, Mao S, Li H, Wang Y. Highly uniform Ru nanoparticles over N-doped carbon: pH and temperature-universal hydrogen release from water reduction. Energy Environ Sci 2018;11:800–6.
[61] Su J, Yang Y, Xia G, Chen J, Jiang P, Chen Q. Ruthenium-cobalt nanoalloys encapsulated in nitrogen-doped graphene as active electrocatalysts for producing hydrogen in alkaline media. Nat Commun 2017;8:14969.
[62] Jiang P, Yang Y, Shi R, Xia G, Chen J, Su J, Chen Q. Pt-like electrocatalytic behavior of Ru–MoO_2 nanocomposites for the hydrogen evolution reaction. J Mater Chem A 2017;5:5475–85.
[63] Liu Y, Liu S, Wang Y, Zhang Q, Gu L, Zhao S, Xu D, Li Y, Bao J, Dai Z. Ru modulation effects in the synthesis of unique rod-like Ni@Ni2P–Ru heterostructures and their remarkable electrocatalytic hydrogen evolution performance. J Am Chem Soc 2018;140:2731–4.
[64] Xu Y, Yin S, Li C, Deng K, Xue H, Li X, Wang H, Wang L. Low-ruthenium-content NiRu nanoalloys encapsulated in nitrogen-doped carbon as highly efficient and pH-universal electrocatalysts for the hydrogen evolution reaction. J Mater Chem A 2018;6:1376–81.
[65] Barman BK, Sarkar B, Nanda KK. Pd-coated Ru nanocrystals supported on N-doped graphene as HER and ORR electrocatalysts. Chem Commun 2019;55:13928–31.

[66] Li J-S, Li J-Y, Huang M-J, Kong L-X, Wu Z. Anchoring RuxP on 3D hollow graphene nanospheres as efficient and pH-universal electrocatalysts for the hydrogen evolution reaction. Carbon 2020;161:44–50.
[67] Yang H, Tang Z, Wang K, Wu W, Chen Y, Ding Z, Liu Z, Chen S. Co@Pd core-shell nanoparticles embedded in nitrogen-doped porous carbon as dual functional electrocatalysts for both oxygen reduction and hydrogen evolution reactions. J Colloid Interface Sci 2018;528:18–26.
[68] Chen Y, Peng J, Duan W, He G, Tang Z. NiFe alloyed nanoparticles encapsulated in nitrogen doped carbon nanotubes for bifunctional electrocatalysis toward rechargeable Zn-air batteries. ChemCatChem 2019;11:5994–6001.
[69] Tabassum H, Mahmood A, Zhu B, Liang Z, Zhong R, Guo S, Zou R. Recent advances in confining metal-based nanoparticles into carbon nanotubes for electrochemical energy conversion and storage devices. Energy Environ Sci 2019;12:2924–56.